Dynamic modeling of hyper-elastic soft robots using spatial curves

Available online at www.sciencedirect.com

ScienceDirect

IFAC PapersOnline CONFERENCE PAPER ARCHIVE

IFAC PapersOnLine 53-2 (2020) 9238–9243

Dynamic modeling of hyper-elastic soft robots using spatial curves

Brandon J. Caasenbrood * **Alexander Y. Pogromsky** *,** **Henk Nijmeijer** *

* *Mechanical Engineering Department, Eindhoven University of Technology, Eindhoven, The Netherlands (e-mail: b.j.caasenbrood@tue.nl, a.pogromski@tue.nl, h.nijmeijer@tue.nl)*
** *Department of Control Systems and Informatics, Saint-Petersburg National Research University of Information Technologies, Mechanics, and Optics (ITMO), Russian Federation*

Abstract: Soft robots differ fundamentally from traditional robotics. Due to their composition of soft materials, soft robots are inherently compliant and allow for large continuum-bodied motion. Although some frameworks exist for describing the kinematics, the development of dynamic models intended for control-oriented applications is relatively scarce and, to some extent, underdeveloped. This paper provides a modeling framework to describe the nonlinear dynamics of a soft robot using differential geometry of spatial curves. Furthermore, we include the geometrically nonlinear and time-variant mechanical nature imposed by these soft materials into our modeling framework. Numerical simulations of the dynamic model are presented, as well as experimental validations of a study case soft robot to illustrate the accuracy. The proposed modeling framework can be used to simulate the nonlinear dynamics of soft robots but also to calculate the inverse dynamics required for model-based control.

Keywords: Modeling, Robots manipulators, Robotics technology.

1. INTRODUCTION

In recent years, the area of soft robotics is gaining attention amongst the scientific community, focusing on developing compliant and lightweight robots composed of 'softer' materials like silicone rubbers. Unlike traditional robots, whose rigidity strives for precision and repeatability, the morphology of soft robots arises from their flexible mechanical structure that, to some degree, resemblances the mobility and robustness found in nature. Consequently, researchers often attempt to fabricate soft robots by mimicking the compliance and morphology of living creatures, resulting in a diverse class of bio-inspired robots, e.g., Marchese et al. (2014); Falkenhahn et al. (2015). The use of hyper-elastic materials enables soft robots to accomplish incredible features with relative ease, e.g., adaptive grasping as shown in Galloway et al. (2016); Kim et al. (2013), and terrestrial and aquatic locomotion in Drotman et al. (2017); Choi et al. (2011). Soft robotics posses several advantages over their rigid counterparts, including weight, affordability, and safety in human-robot interaction. Despite recent advancements, however, soft robots are often controlled in open-loop or through teleoperations; and unlike rigid robotics, systematic frameworks for deriving accurate dynamic models intended for model-based control strategies are still lacking.

With the introduction of soft robotics, conventional approaches used to model the dynamics become less convenient. In contrast to its rigid counterpart, soft robots theoretically have an infinite number of degrees-of-freedom; consequently, describing the kinematics while moderating complexity becomes increasingly more challenging. Soft robotics differ from hyper-redundant robotics as their continuously deformable-body lacks joints and links. Hence, they constitute a class of continuum robots. Some kinematic frameworks include the work of Jones (2006) that describes spatially-constant curved continuum; the framework of Chirikjian and Burdick (1994) describing continuum structures using modal shape functions, and the work of Mochiyama and Suzuki (2002) providing a general framework for a class of (inextensible) hyper-flexible robot manipulators.

Fig. 1. Soft robot manipulator module entirely 3D-printed from a soft and flexible polyamide material.

Although their kinematics is relatively well-understood, little research is focused on modeling both the hyper-flexibility and the nonlinear (time-varying) dynamics regarding the deformation of soft materials, which might stem from a perceived multidisciplinary gap between the

10.1016/j.ifacol.2020.12.2209

fields of control and continuum mechanics. Soft mechanical structures require accurate models to both describe the static and dynamic nature under large deformations, and the hyper-elastic and visco-elastic material behavior in control-oriented research is often neglected. As of this day, model-based control strategies in soft robotics are still scarce, and many researchers employ linear control methodologies (e.g., PD or PID). Ultimately, the strong nonlinearities in soft robotics encourage the use of model-based strategies, like computed-torque controllers. Unfortunately, model-based approaches issue the trade-off between accuracy and complexity. To reduce model complexity in these highly-nonlinear systems, some researchers exploit machine learning techniques, including Thuruthel et al. (2017); Runge et al. (2017); Nakajima et al. (2018). Others use snapshot methods of finite element simulations, Coevoet et al. (2017); Thieffry et al. (2017), or mass-lumped models, Falkenhahn et al. (2015). Yet, ultimately, systematic and general modeling approaches applicable to a wide range of soft robots and soft materials are still lacking, whereas a large number of models are likely not suited for model-based control.

In this work, we provide a systematic framework to model the dynamics of a class of soft robotics, namely soft robot manipulators. To describe their continuum-bodied motion, we exploit the differential geometric properties of spatial curves. In addition, the hyper- and visco-elastic nature of the soft robot is described in terms of the curve kinematics whose stiffness identification is obtained through finite element methods. As a study case, we fabricated a soft robot manipulator that is fully 3D-printed, as shown in Fig. 1. The soft robot and its dynamic model is made publicly available (see Caasenbrood (2019)). The soft robot is composed of printable polyamide material with a relatively low Young's modulus ($\leq$ 80 MPa). The soft robot is printed through a printing process called Selective Laser Sintering, which ensures high detail for complex geometries. The soft robot has three (independent) pneumatic bellows, and by inflation or deflation of these embedded bellows, the elastic body is capable of elongation and omnidirectional bending.

The organization of this work is as follows. In section 2, we describe a framework for modeling the dynamics of a hyper-flexible soft robot, followed by a material analysis in section 3. Then, the simulation results of the proposed model and the experimental validation will be discussed in section 4, followed by a brief conclusion in section 5.

2. DYNAMIC MODEL OF SOFT ROBOT

2.1 Kinematic representation

Let the deformation of the hyper-elastic body be represented by a generalized coordinate vector $q(t) \in \mathbb{R}^n$ with n the number of degrees-of-freedom. To represent the posture of the soft robot, we introduce a smooth one-dimensional curve passing through the geometric center of soft robot (see Fig. 2). This spatial curve maps a spatial parameter $\sigma \in \mathbb{R}$ and a generalized coordinate vector $q(t)$ to a position vector in $\mathbb{R}^3$, that is,

$$p : \mathbb{R}^n \times \mathbb{R} \mapsto \mathbb{R}^3. \tag{1}$$

We refer to this spatial curve as the backbone of the soft robot, since it depicts the geometric deformation of

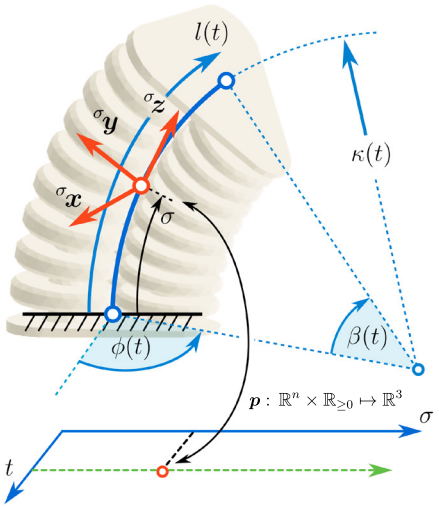

Fig. 2. Curve geometry for the soft robot expressed in the state vector $q(t)$ and its geometrical mapping p

the elastic body. Next, suppose that the parameter σ can evolve on a bounded domain $\sigma \in [0, l]$ with $l(t) \in \mathbb{R}_{>0}$ the extensible arc-length of the soft robot. Then, given any instance $t \in \mathbb{R}_{\geq 0}$, the set $\mathcal{P} = \{p \in \mathbb{R}^3 \mid \sigma \in [0, l]\}$ describes the full configuration of the soft robot. In this work, we model the spatial configurations of the soft robot according to the Piece-wise Constant Curvature condition (PCC). The PCC condition implies that the curvature is spatially independent, and thus the curvature depends exclusively on time, i.e., $\kappa(\sigma, t) = \kappa(t)$. The PCC condition has been proven to be remarkably consistent while avoiding kinematic complexity (e.g., Marchese and Rus (2016); Falkenhahn et al. (2015)). From the PCC condition, we can express the generalized coordinates for the soft robot

$$q(t) = \begin{pmatrix} l & \kappa_x & \kappa_y \end{pmatrix}^\top, \tag{2}$$

where $l(t)$ is the arc-length, and $\kappa_x(t), \kappa_y(t) \in \mathbb{R}$ the curvatures in the x-z and y-z plane, respectively. Although the choice of generalized coordinates is not unique since the soft body has no well-defined joints, we detail the importance on this particular choice of $q(t)$ later in this section.

For each particular point σ on the backbone curve, we introduce an extended Frenet frame described by the orientation matrix $\Phi(q, \sigma) \in SO(3)$, belonging to the group of special orthogonal matrices. The expression for the orientation matrix of the Frenet frame ${}^0\Phi(q, \sigma)$ viewed from the base frame is given by

$${}^0\Phi(q, \sigma) = \begin{pmatrix} {s_\phi}^2 v_a + c_a & -s_\phi c_\phi v_a & c_\phi s_a \\ -c_\phi s_\phi v_a & {c_\phi}^2 v_a + c_a & s_\phi s_a \\ -c_\phi s_a & -s_\phi s_a & c_a \end{pmatrix}, \tag{3}$$

with abbreviated notations $c_a = \cos(\sigma\kappa)$, $s_a = \sin(\sigma\kappa)$, $v_a = 1 - c_a$, $c_\phi = \cos(\phi)$ and $s_\phi = \sin(\phi)$ with $\phi = \operatorname{atan2}(\kappa_y, \kappa_x)$ the orientation angle, $\kappa = ({\kappa_x}^2 + {\kappa_y}^2)^{1/2}$ the net curvature. The position vector for any point σ on the backbone curve can be obtained by spatial integrations of the tangent vector along the backbone, that is,

$${}^0p(q, \sigma) = \int_0^\sigma {}^0\Phi(q, \eta)\, e_z \, d\eta, \tag{4}$$

where $e_z = (0\ 0\ 1)^\top$. Before deriving the kinematics, let us first introduce some coordinate transformations

$$^{\xi}\Phi(q,\sigma) := {}^{0}\Phi(q,\xi)^\top {}^{0}\Phi(q,\sigma), \tag{5}$$

$$^{\xi}p(q,\sigma) := {}^{0}\Phi(q,\xi)^\top {}^{0}p(q,\sigma), \tag{6}$$

for any $\xi, \sigma \in \mathbb{R}$. The expressions (4) and (5) allow us to transition between different coordinate frames on the smooth backbone curve. Second, we introduce the mapping $[\,\cdot\,]_\times$ as the isomorphism between $\mathbb{R}^3$ and $so(3)$, i.e. the Lie algebra of the group $SO(3)$. Specifically, given a vector $v \in \mathbb{R}^3$, $[v]_\times$ denotes the skew-symmetric matrix that satisfies $[v]_\times w = v \times w$ for all $w \in \mathbb{R}^3$. According to Mochiyama and Suzuki (2002), the spatial derivative of the orientation matrix ${}^{0}\Phi(q,\sigma) \in SO(3)$ can be written as

$$\frac{\partial}{\partial \sigma}\left({}^{0}\Phi(q,\sigma)\right) = {}^{0}\Phi(q,\sigma)\left[\theta(q,\sigma)\right]_\times, \tag{7}$$

where $[\theta(q,\sigma)]_\times \in \mathbb{R}^{3\times 3}$ is a skew-symmetric matrix with $\theta(q,\sigma) \in \mathbb{R}^3$ a unique vector satisfying (7). The vector θ is referred to as the frame-rate vector as its entries represent the angular change between frames regarding a change in σ. Given this geometric notion of the angular change, the Jacobian of the frame-rate vector is defined by

$$J_\omega := \frac{\partial \theta}{\partial q} = \begin{pmatrix} 0 & 0 & -1 \\ 0 & 1 & 0 \\ 0 & 0 & 0 \end{pmatrix}. \tag{8}$$

In literature, the Jacobian J_ω is also called the rotational axis matrix as its columns correspond to the joint axis of rotation. Here, we stress the importance of the choice of generalized coordinates as in (2) since Jacobian matrix J_ω naturally arises as a constant matrix iff the joint axes coincide with the axes of the Frenet frames. Regarding translation kinematics, we introduce a body-rate vector $h = (0\ \ 0\ \ \varepsilon)^\top$ with $\varepsilon(q) := l - l_0$, which represents the local translational change due to extensibility of the soft robot. The Jacobian of the body-rate vector is referred to as the translational axis matrix whose columns represent the joint axis of translation. Its Jacobian is defined by

$$J_v := \frac{\partial h}{\partial q} = \begin{pmatrix} 0 & 0 & 0 \\ 0 & 0 & 0 \\ 1 & 0 & 0 \end{pmatrix}. \tag{9}$$

Let $V(q,\sigma) \in \mathbb{R}^6$ be a concatenated vector of the linear velocities and angular velocities for a particular point σ. Then, we can express the twist for any point σ on the backbone curve as follows

$$V(q,\dot{q},\sigma) = \int_0^\sigma Ad_r(q,\sigma,\eta)\, J^*\, \dot{q}\, d\eta, \tag{10}$$

where $Ad_r(q,\sigma,\eta) \in \mathbb{R}^{6\times 6}$ is the adjoint transformation matrix, and $J^* = \left(J_v^\top, J_\omega^\top\right)^\top$ the concatenation of the time-invariant Jacobians in (8) and (9). More specifically, the adjoint transformation in (10) maps the twist velocity vector from the coordinate frame corresponding to η onto the coordinate frame corresponding to σ. The adjoint transformation matrix in terms of a rigid body transformation between η and σ is described by

$$Ad_r(q,\sigma,\eta) := \begin{pmatrix} {}^{\sigma}\Phi(q,\eta) & [r(q,\sigma,\eta)]_\times\, {}^{\sigma}\Phi(q,\eta) \\ 0_3 & {}^{\sigma}\Phi(q,\eta) \end{pmatrix}, \tag{11}$$

where $r(q,\sigma,\eta) = {}^{\sigma}p(q,\eta) - {}^{\sigma}p(q,\sigma)$ is the relative position vector of frame η viewed from the frame at σ.

2.2 Dynamic model

From the kinematic relation in (10), we can further assess the dynamics of the soft robot using the Euler-Lagrange equation of motion, that is,

$$\frac{\partial}{\partial t}\frac{\partial \mathcal{L}}{\partial \dot{q}} - \frac{\partial \mathcal{L}}{\partial q} = Q^{nc}, \tag{12}$$

where the Lagrangian is defined by $\mathcal{L}(q,\dot{q}) := \mathcal{T}(q,\dot{q}) - \mathcal{V}(q)$, respectively the difference between kinetic and potential energy, and Q^{nc} the generalized non-conservative forces. To obtain the dynamics for a hyper-flexible continuum-bodied solid, suppose each point σ on the curve $p(q,\sigma)$ corresponds to an infinitesimal slice of the continuum body. Given this notion, the inertia tensor for such an infinitesimal body at point σ can be written as

$$M(q) = \mathrm{diag}\left(m_\sigma,\, m_\sigma,\, m_\sigma,\, I_\sigma\right), \tag{13}$$

where $m_\sigma(q) = m_0/l(q)$ is the mass line density, $I_\sigma(q) \in \mathbb{R}^{3\times 3}$ the area moment of inertia tensor, and the operator $\mathrm{diag}(\cdot)$ forms a block diagonal matrix. In this work, the inertial properties of the infinitesimal slices can be approximated by a flat disk of radius r with mass $m_\sigma(q)$. Now, the total kinetic energy function of the soft robot manipulator can be written as

$$\mathcal{T}(q,\dot{q}) = \frac{1}{2}\int_0^l V(q,\dot{q},\sigma)^\top M(q)\, V(q,\dot{q},\sigma)\, d\sigma. \tag{14}$$

Similarly, for the potential energy function describing the elastic and gravitational potential forces, we can write

$$\mathcal{V}(q) = \int_0^l m(q)\, {}^{0}g^\top {}^{0}p(q,\sigma)\, d\sigma + \int_0^\varepsilon k_e(\eta)\eta\, d\eta + \int_0^\beta k_b(\eta)\eta\, d\eta, \tag{15}$$

where ${}^{0}g \in \mathbb{R}^3$ the gravitational acceleration vector, $\beta(q) := \kappa l$ the bending angle of the end-effector, and $k_b : \mathbb{R} \mapsto \mathbb{R}_{>0}$ and $k_e : \mathbb{R} \mapsto \mathbb{R}_{>0}$ respectively describe the nonlinear elongation and bending stiffness imposed by the hyper-elastic material and nonlinear geometrical deformations of the elastic body. It shall be clear that these stiffness functions are nonlinear, possibly time-variant, and they are unique for each soft robotic system due to its dependency on in geometry and material composition. In section 3, we will further detail the hyper-elasticity and visco-elasticity of elastomer materials.

By substitution of the Lagrangian into (12) the Euler-Lagrange equations of motion can be written in the form

$$D(q)\ddot{q} + C(q,\dot{q})\dot{q} + N(q) + F(\dot{q}) = \tau(t) + \tau_{ext}(t) \tag{16}$$

where $D(q) \in \mathbb{R}^{3\times 3}$ is the inertia matrix, $C(q,\dot{q}) \in \mathbb{R}^{3\times 3}$ the centripetal-Coriolis matrix, $N(q) \in \mathbb{R}^3$ the vector related to the gravitational and elastic potential forces, $F(\dot{q}) = R\dot{q}$ the vector related to the dissipative forces with positive definite matrix $R \in \mathbb{R}^{3\times 3}$, and τ and τ_{ext} are the input forces and external disturbance forces, respectively. In conventional soft robotics, the external forces $\tau(t)$ are realized through pneumatic or hydraulic actuation. The dynamic model of the soft robot is assembled using the `MATLAB/Symbolic Toolbox`, and the source code is made publicly available at Caasenbrood (2019).

3. MATERIAL MODEL FOR ELASTOMERS

3.1 Hyper-elastic stiffness

As mentioned previously, the key difference between traditional robotics and soft robotics is that soft robotics exploit their flexible morphology to accomplish mobility. Consequently, soft structures undergo large (reversible) deformation by virtue of their low elasticity. The presence of large deformations and rubber-like materials inherently leads to state-dependency in the mechanical compliance of the solid, and thus Hooke's law for linear elasticity no longer holds. As previously discussed, the hyper-elasticity and the nonlinear geometrical deformations of the soft robot can be characterized by a nonlinear stiffness function. To ensure that these nonlinear stiffness functions are well-posed, we impose the following conditions for the elongation and bending stiffness:

(1) $\exists \underline{k}, \bar{k} \;\; \underline{k} \leq k_i(x) \leq \bar{k} \; \forall x \in \mathbb{R}$,
(2) $k_i(x)$ is strictly convex with $\operatorname{argmin} k_i(x) = 0$,

with subscript $i \in \{e, b\}$ denoting the bending and elongation elasticity, respectively. Condition 2) is a necessary condition as it inhibits any elasto-plastic behavior, i.e., elastic bodies undergoing non-reversible deformation due to applied forces. Hence, we propose the following ansatz for the hyper-elastic stiffness model:

$$k_e(\varepsilon, \alpha) = \alpha_1 + \alpha_2 \left[\tanh(\alpha_3 \varepsilon)^2 - 1\right], \tag{17}$$

$$k_b(\beta, \alpha) = \alpha_1 + \alpha_2 \left[\tanh(\alpha_3 \beta)^2 - 1\right], \tag{18}$$

where $\alpha_i \in \mathbb{R}$ for $i \in \{1, 2, ..., 6\}$ are stiffness parameters. The nonlinear contributions in (17) and (18) represent strain-hardening of the elastomer material. To satisfy the stiffness conditions mentioned above, it should hold that $\alpha_1 > \alpha_2$, $\alpha_4 > \alpha_5$, and $\alpha_{3,6} > 0$.

From static input-output behavior, i.e., the relationship between applied pressure and generalized deformation, we can identify the hyperelasticity material parameters α. It shall be clear that this quasi-static relation can be obtained experimentally, however, due to complexity under large deformation, finite element analysis was preferred. The finite element simulations are performed using `Abaqus/CAE`, a finite element solver. Here, we used an incompressible neo-Hookean material model. To our knowledge, the 3D-printed polyamide material is linear isotropic with Young's modulus $E = 80$ MPa and a Poisson ration $\nu = 0.49$. In accordance to linear elasticity, the neo-Hookean material constant is $C_1 = E/4(1 + \nu)$. The numerical simulations also include (tangent) self-contact to better reflect the actuation limits. The mapping from differential pressure to actuation force/torque can be obtained via geometric analysis. The least-squares nonlinear regression results for both the elongation stiffness $k_e(\varepsilon, \alpha)$ and bending stiffness $k_b(\beta, \alpha)$ are shown in Fig. 3. Note that the regression is slightly biased towards the positive strain regime, to better represent the stiffness under positive differential pressure. The material parameters are given in Table 1.

Table 1. Estimated material parameters.

	$i=1$	$i=2$	$i=3$	$i=4$	$i=5$	$i=6$
α_i	2.23e+3	1.74e+3	-4.55e+2	4.23e-1	3.99e-1	-2.29e-1
γ_i	3.21e+2	5.22e-1	2.84e+2	1.82e-3	2.84e+2	1.82e-3

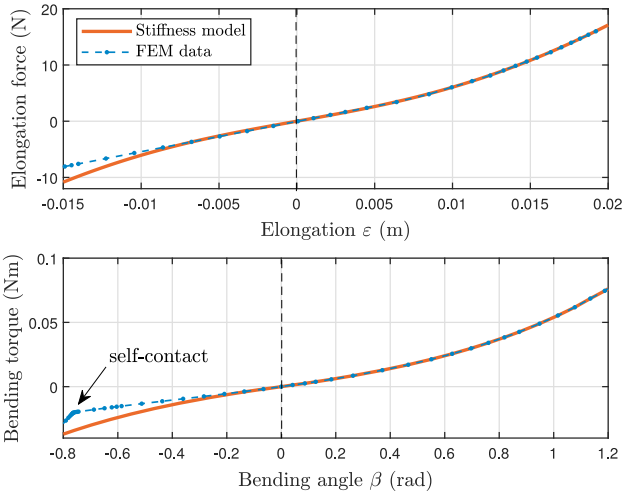

Fig. 3. Regression results of the elongation stiffness and bending stiffness driven by finite element analysis.

3.2 Visco-elasticity

Unlike ideal elastic materials, polymer materials (typically) inhibit abrupt change in stress, since the material evenly disperses the stress concentration within the polymer chain network at a slower rate relative to the applied strain rate. This phenomenon of the stress dispersion is called creep, and we characterize this viscous behavior by introducing a new state vector $\lambda(t) \in \mathbb{R}^3$, the creeping strains. From Meyers and Chawla (2008), the Kelvin-Voigt model for creep can be described by a first-order ordinary differential equation of the form:

$$\dot{\lambda}_i(t) = -\gamma_{(2i-1)}\lambda_i - \gamma_{(2i)}\dot{q}_i, \tag{19}$$

where the vector $\gamma = (\gamma_1, \gamma_2, ..., \gamma_6)^\top$ represents a vector of visco-elastic material parameters, and the state variables $\lambda_i(t)$ with $i \in \{1, 2, 3\}$, i.e., the creep strains. Here, the visco-elasticity can be intuitively included into (16) as an external disturbance force τ_{ext}, that is, $\tau_{ext} = K^\top \lambda$ with K a compliance matrix, which maps the creep strains to forces. Since creeping strains are difficult, if not impossible, to distinguish from the true strain in experimental data, their corresponding material parameters γ and the compliance K are determined empirically (e.g., unforced oscillations). The estimated material parameters for the visco-elastic dynamics are given in Table 1. It is worth mentioning that the initial conditions for the creeping strains $\lambda(t_0)$ are also determined a priori.

4. NUMERICAL ANALYSIS

4.1 Simulation Model

In this section, we perform numerical simulations of the dynamical model detailed in (16). The purpose of the simulations is twofold, namely, to investigate the dynamic behavior of the model and to verify the model experimentally. The solutions of the ordinary differential equation in (16) are obtained through an explicit time-integration scheme (`ode45.m`), in which the timesteps are set at $\Delta t = 1$ ms. For the remainder of this section, we denote the initialization of the states variables as $q(t_0) = q_0$ and $\dot{q}(t_0) = \dot{q}_0$. We choose the following physical properties for the soft robot

study case: the mass $m = 49.4$ g, the undeformed arc-length $l_0 = 64.4$ mm, and the radius of the cross-sections $r = 23.5$ mm. The material parameters for hyper-elasticity and visco-elasticity model are chosen according to Table 1, and the creep compliance is $K = \text{diag}\{k_1, k_2, k_3\}$ with $k_1 = 502.3$ N/m and $k_2 = k_3 = 1.53 \cdot 10^{-2}$ Nm. Furthermore, we choose $R = \text{diag}(c_1, c_2, c_3)$ with coefficients $c_1 = 0.12$ Ns/m and $c_2 = c_3 = 5.93 \cdot 10^{-7}$ Nms. The simulation code is made available at Caasenbrood (2019).

4.2 Simulations and model validation

We first investigate the dynamics of the unforced system. By examining the gradient of the potential energy function $\mathcal{V}(q)$, we conclude the existence of one stable set of equilibria and one unstable equilibrium. The potential energy has a local maximum for the solution $(l, \kappa_x, \kappa_y) = (l_0 - mg/\alpha_3, 0, 0)$, which is the upright position of the soft manipulator. Furthermore, by using the bisection method to find the zero-crossing of the gradient of the potential function, we find that all stable solutions tend to the set $\Omega = \left\{ q \in \mathbb{R}^3 \ : \ l = 0.0635, \ \sqrt{\kappa_x^2 + \kappa_y^2}) = 0.1737 \right\}$, which corresponds to the hanging position of the soft robot. This stable set of equilibria arises from the balance between the gravitational and elastic potential force.

To show the existence of stable solutions, we simulated the dynamic model with non-zero initial conditions. The following non-zero initial conditions are chosen $q_0 = [0.064, 25, 0]^\top$ and $\dot{q}_0 = [0, 0, 1500]^\top$. The simulation results are shown in Fig. 4 and Fig. 5, where we show respectively the state trajectories and the trajectories of the end-effector (i.e., $\sigma = l(t)$). As can be seen, the state solutions will orbit around the stable equilibrium, and, due to dissipation, they eventually converge to the set Ω. Besides the existence of stable solutions, the numerical results illustrate the coupled dynamics between the elongation and bending of the soft robot. Due to the difference in mechanical stiffness for elongation and bending, we observe high-frequency and low-frequency oscillation for the length $l(t)$, whereas we solely observe low-frequency oscillations for the curvatures $\kappa_x(t)$ and $\kappa_y(t)$. Regarding the elongation dynamics, the high-frequency oscillations in $l(t)$ are directly coupled to the large elongation stiffness. In contrast, the low-frequency oscillations are passed from the curvature dynamics to length dynamics; conversely, the dynamics of the elongation barely affect the curvatures.

To show the validity of the proposed dynamic model, we compare the measured state trajectories of the physical soft robot to simulated trajectories with similar initial conditions. We like to stress that sensing for soft robotics is rather challenging, due to their large deformations and hyper-flexibility. Instead of measuring the full state information q and $\dot{q}$ directly, an inertial measurement unit (BNO055) is used to measure the angular response of the end-effector (i.e., corresponding to $\sigma = l(t)$). Using a sensor-fusion approach, the bending angle of the soft robot can be recovered, i.e., $\beta = \kappa l$.

For the validation, two experimental trails are considered. In the first experiment, the soft robot is deformed slightly and then released from rest, which correspond to the initial conditions $q_0 = [\, 0.065, 4.75, 0 \,]^\top$ and $\dot{q}_0 = 0_3$. Since

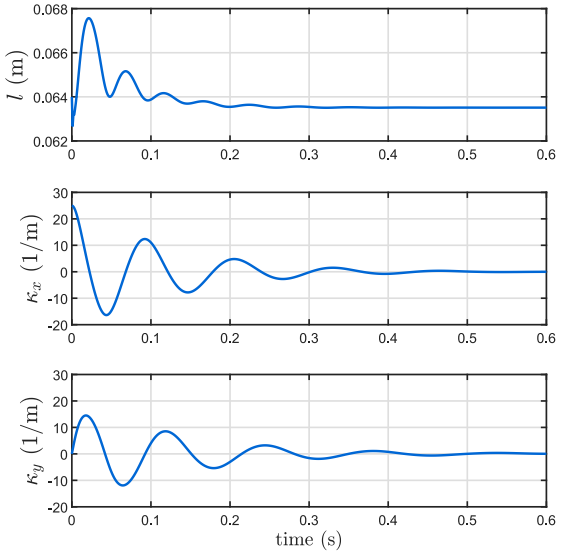

Fig. 4. State trajectories of simulated dynamics of the soft robot manipulator with initial conditions $q_0 = [0.064, 25, 0]^\top$ and $\dot{q}_0 = [0, 0, 1500]^\top$.

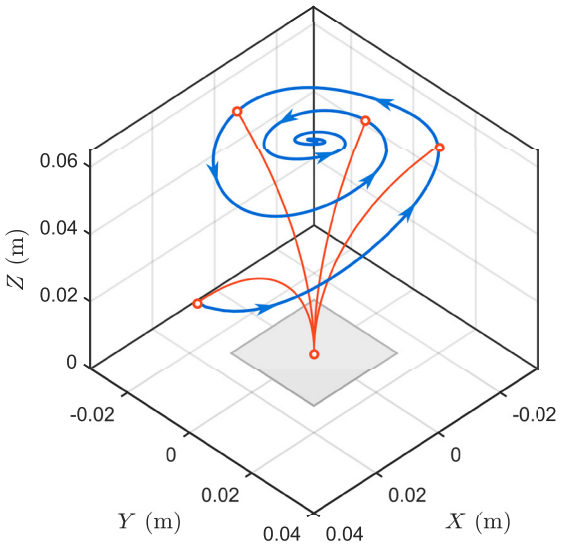

Fig. 5. Three dimensional representation of end-effector trajectories from the soft robot model.

the robot is deformed slightly, the hyper-elasticity and visco-elasticity material behavior become less apparent. In the second case, the soft robot is deformed within the nonlinear visco-elastic regime and then released from rest, which corresponded with the following initial conditions $q_0 = [\, 0.067, 11.25, 0 \,]^\top$ and $\dot{q}_0 = 0_3$. Here, the nonlinear and time-dependent material effects cannot be neglected. Since the creep strains λ are indistinguishable from the true strain, optimal initial conditions for $\lambda(t_0)$ are determined empirically. The validation results are shown in Fig. 6.

From the validation results, we observe that the state trajectories of the end effector closely match the true trajectories, even for significant (nonlinear) deformations. For the first case (inside linear elastic regime), the RMS error and the maximum error is ± 0.19 and ± 0.50 deg, respectively. For the second case (outside the linear elastic

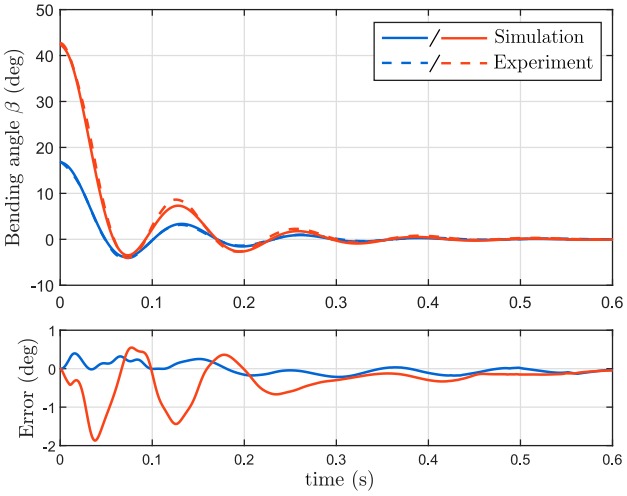

Fig. 6. Validation results for the dynamic model, where the dashed lines represent the experimental data from the IMU and the solid lines the simulated trajectories.

regime), the RMS error and the maximum error is ± 0.55 and ± 1.84 deg, respectively.

5. CONCLUSION

In this paper, we provided a theoretical framework to model the kinematics and the dynamics of soft robot manipulators composed of elastomer material. By modeling the soft robotic body as a constant-curvature spatial curve, the nonlinear geometric deformation of the hyper-flexible body can be represented, and the continuum-body kinematics can be derived analytically. Given the kinematic model, a nonlinear dynamic model of a hyper-flexible soft robot manipulator can be obtained using the Euler-Lagrange equations. The validity of the proposed approach is demonstrated by comparing the state trajectories of the physical soft robot and its representative dynamic model, showing a significantly small discrepancy between the model and the physical system. The advantage of the approach is its flexibility to suit various soft robotic systems undergoing similar continuum-body deformations (e.g., soft grippers, artificial muscles, fish-tails) and therefore eliminating the need for complex or computational expensive changes to the dynamic model. In future work, the proposed modeling approach could be used for other soft robotic systems, and the model could be used for the synthesis of model-based controllers, e.g., computed-torque controllers.

ACKNOWLEDGEMENTS

This work was supported by NWO, Netherlands Organization for Scientific Research; and is part of the Wearable Robotics perspective program.

REFERENCES

Caasenbrood, B. (2019). Dynamic modeling of soft robots for matlab. https://github.com/BJCaasenbrood/soft-robotics-MATLAB.

Chirikjian, G.S. and Burdick, J.W. (1994). Hyper-redundant manipulator. *IEEE Robotics and Automation Magazine*, 1(4), 22–29.

Choi, W., Whitesides, G.M., Wang, M., Chen, X., Shepherd, R.F., Mazzeo, A.D., Morin, S.A., Stokes, A.A., and Ilievski, F. (2011). Multigait soft robot. *Proceedings of the National Academy of Sciences*, 108(51), 20400–20403.

Coevoet, E., Morales-Bieze, T., Largilliere, F., Zhang, Z., Thieffry, M., Sanz-Lopez, M., Carrez, B., Marchal, D., Goury, O., Dequidt, J., and Duriez, C. (2017). Software toolkit for modeling, simulation, and control of soft robots. *Advanced Robotics*, 31(22), 1208–1224.

Drotman, D., Jadhav, S., Karimi, M., Dezonia, P., and Tolley, M.T. (2017). 3D printed soft actuators for a legged robot capable of navigating unstructured terrain. *Proceedings - IEEE International Conference on Robotics and Automation*, 5532–5538.

Falkenhahn, V., Mahl, T., Hildebrandt, A., Neumann, R., and Sawodny, O. (2015). Dynamic Modeling of Bellows-Actuated Continuum Robots Using the Euler-Lagrange Formalism. *IEEE Transactions on Robotics*, 31(6), 1483–1496.

Galloway, K.C., Becker, K.P., Phillips, B., Kirby, J., Licht, S., Tchernov, D., Wood, R.J., and Gruber, D.F. (2016). Soft Robotic Grippers for Biological Sampling on Deep Reefs. *Soft Robotics*, 3(1), 23–33.

Jones, B. and Walker, I. (2006). Kinematics for multisection continuum robots. *IEEE Transactions on Robotics*, 1, 43–55.

Kim, S., Laschi, C., and Trimmer, B. (2013). Soft robotics: A bioinspired evolution in robotics. *Trends in Biotechnology*, 31(5), 287–294.

Marchese, A.D., Onal, C.D., and Rus, D. (2014). Autonomous Soft Robotic Fish Capable of Escape Maneuvers Using Fluidic Elastomer Actuators. *Soft Robotics*, 1(1), 75–87.

Marchese, A.D. and Rus, D. (2016). Design, kinematics, and control of a soft spatial fluidic elastomer manipulator. *The International Journal of Robotics Research*, 35(7), 840–869. doi:10.1177/0278364915587925.

Meyers, M. and Chawla K. (2008). *Mechanical Behavior of Materials*. Cambridge University Press, New York.

Mochiyama, H. and Suzuki, T. (2002). Dynamical modelling of a hyper-flexible manipulator. *Proceedings of the 41st SICE Annual Conference. SICE 2002.*, 3. doi: 10.1109/SICE.2002.1196530.

Nakajima, K., Hauser, H., Li, T., and Pfeifer, R. (2018). Exploiting the Dynamics of Soft Materials. *Soft Robotics*, 5(3), 339–347.

Runge, G., Wiese, M., and Raatz, A. (2017). FEM-Based Training of Artificial Neural Networks for Modular Soft Robots.

Spong, M.W., Hutchinson, S., and Vidyasagar, M. (2006). *Robot modeling and control*. Jonn Wiley and Sons, inc., New York.

Thieffry, M., Kruszewski, A., Goury, O., Guerra, T.M., and Duriez, C. (2017). Dynamic Control of Soft Robots. *IFAC World Congress*.

Thuruthel, T.G., Falotico, E., Renda, F., and Laschi, C. (2017). Learning dynamic models for open loop predictive control of soft robotic manipulators. *Bioinspiration and Biomimetics*, 12(6).